**KU LEUVEN**

# IDEAS.mo

## Integrated District Energy Assessment Simulations

Ruben Baetens, Roel De Coninck, Bart Verbruggen, Juan Van Roy,
Johan Driesen, Lieve Helsen, Dirk Saelens

# CONTENTS

# I
## SPECIFICATIONS

# Chapter 1

# CLIMATE

In this section, we describe in detail the climate model and its possibilities that are implemented in Modelica as part of the IDEAS platform. Four external factors are to be known, i.e. external temperature and ground temperature for transient heat losses by conduction, sky temperature for long-wave radiation losses and short-wave gains on surfaces by solar irradiation.

## 1.1 Climate conditions

In this section, we describe in detail the climate model and its possibilities that are implemented in Modelica as part of the IDEAS platform. Four external factors are to be known, i.e. external temperature and ground temperature for transient heat losses by conduction, sky temperature for long-wave radiation losses and short-wave gains on surfaces by solar irradiation.

### 1.1.1 Weather data

The main weather parameters required for transient thermal building simulation are the ambient dry-bulb temperature $T_{db}(t)$, the outdoor relative humidity $\varphi_e(t)$, the wind speed $v_{10}(t)$, the diffuse horizontal solar radiation $E_{d,h}(t)$ and direct normal solar radiation $E_{D,\perp}(t)$.

The Meteonorm system[1] is a comprehensive source of (all mentioned) weather data for engineering applications in Europe and this system is used within this context. For simulation, the retrieved data from the Meteonorm system are not used within the common formats of a test reference year `*.try`[2;3] as used in Europe or the formats of a typical meteorological years `*.tmy` or `*.tmy2`[4?] and weather years for energy calculations `*.wyec` or `*.wyec2`[5] as used in the United States and Canada. These data formats are derived from hourly observations at a specific location by the national

weather service or meteorological office and contain too little information for sub-hourly simulation, especially towards renewable energy generation by solar radiation.

From the retrieved data from the Meteonorm system, one more temperature needs to be determined. The long-wave radiative heat exchange of an exterior surface with a cloudy sky is calculated based on a sky temperature. This black-body sky temperature $\boldsymbol{T}_{ce}$ can be determined[6;7] as

$$\boldsymbol{T}_{ce} = \boldsymbol{T}_{db} \sqrt[4]{\varepsilon_{ce}} \tag{1.1}$$

$$\varepsilon_{ce} = \varepsilon_{ce,0} + \boldsymbol{C}_{cf}\boldsymbol{\varsigma}_{ce,0} \tag{1.2}$$

where $\varepsilon_{ce}$ is the cloudy sky emissivity[7-9], where $\varepsilon_{ce,0}$ is the clear sky emisivity and $\boldsymbol{C}_{cf}$ is the cloud cover factor. Both $\varepsilon_{ce,0}$ and $\boldsymbol{C}_{cf}$ are determined as polynomial fits on measurement data:

$$\varepsilon_{ce,0} \propto 0.711 + 0.0056\ \boldsymbol{\vartheta}_{dw} + 0.000073\ \boldsymbol{\vartheta}_{dw}^2 + 0.013\ \cos\boldsymbol{h} \tag{1.3}$$

$$\boldsymbol{C}_{cf} \propto 1.0 + 0.024\ \boldsymbol{C}_c - 0.0035\ \boldsymbol{C}_c^2 + 0.00028\ \boldsymbol{C}_c^3 \tag{1.4}$$

where $\boldsymbol{h}$ is the hour angle, $\boldsymbol{\vartheta}_{dw}$ is the dew temperature and $\boldsymbol{C}_c$ is the tenths cloud cover retrieved from Meteonorm[10;11].

## 1.1.2 Solar radiation

The calculation of the direct and diffuse solar irradiation on a tilted surface requires determination of the position of the sun in the sky. Here, the zenith angle $\xi(t, x)$ of surface with inclination $i(x)$ and azimuth $a(x)$ are able to uniquely define the the solar radiation on a tilted surface based on the determination of the annual and daily solar cycle by means of solar time and declination.

Within the computational model, all solar irradiation calculations are handled in `Commons.Meteo.Solar.RadSol` which is built-in in each surface receiving solar radiation.

**Solar geometry**

The apparant solar time $\boldsymbol{t}_{sol}$ expressed in seconds is based on daily apparent motion of the sun as seen from the earth. Solar noon is defined as the moment when the sun reaches the highest point in the sky. Solar time defined as

$$\boldsymbol{t}_{sol} = \boldsymbol{t}_{std} + 720\pi^{-1}\left(L_{std} - L_{loc}\right) + \boldsymbol{E}_t \tag{1.5}$$

$$\boldsymbol{E}_t = -120\ e\sin\boldsymbol{M} + 60\tan^2\left(\varepsilon/2\right)\sin\left(2\boldsymbol{M} + 2\lambda_p\right) \tag{1.6}$$

where $\boldsymbol{t}_{std}$ is the standard time of the time zone, $L_{std}$ is the reference meridian, $L_{loc}$ is the lcoal meridian and $\boldsymbol{E}_t$ is the equation of time defining the difference between solar

noon and noon of local civil time, $M$ is the mean anomaly relating to the position of the sun to the earth in a Kepler orbit, $\varepsilon$ is the earth obliquity and $\lambda_p$ the ecliptic longitude of the periapsis, *i.e.*, the closest approach of the earth to the sun. Daylight saving time is taken into account within the simulation and corrects $t_{std}$. Daylight saving time starts in the European Economic Community on March $31 - [(5y)/4 + 4]$ mod 7 and ends on October $31 - [(5y)/4 + 1]$ mod 7 where $y$ denotes the year and mod denotes the remainder by division [12].

Before the zenith angle can be calculated, the declination $\boldsymbol{\delta}$ and solar hour angle $\boldsymbol{h}$ is to be defined to fully specify the position of the sun as seen by an observer at a given time. Here, $\boldsymbol{\delta}$ depicts the angle between the solar beam and the equatorial plane, defined [13] as

$$\sin \boldsymbol{\delta} = \sin \varepsilon \cos \left( 2\pi \left( \boldsymbol{n} + 10 \right) n_y^{-1} \right) \tag{1.7}$$

where $\varepsilon$ is the earth obliquity, $n(t)$ is the one-based day number, i.e. 1 for January 1, and $n_y$ is the length in days of the earth revolution equal to 365.25 days. The correction of 10 days is required as winter solstice, i.e. when the apparent position of the sun in the sky as viewed from the Earth reaches its most northern extreme, occurs at December 21.

The hour angle $\boldsymbol{h}$ depicts the angle between between the half plane of the Earth's axis and the zenith and the half plane of the Earth's axis and the given location, defined as

$$\boldsymbol{h} = 2\pi \boldsymbol{t}_{sol} \, 86400^{-1} - \pi \tag{1.8}$$

where $\boldsymbol{t}_{sol}$ is solar time.

Based on $\boldsymbol{\delta}$ and $\boldsymbol{h}$, the zenith angle $\boldsymbol{\xi}^{(k)}$ of a surface $k$ can be uniquely defined. The zenith angle of the sun to a surface is the angle between this surface normal and the sun's beam, and is derived from [14;15]

$$\cos \boldsymbol{\xi}^{(k)} = \sin \boldsymbol{\delta} \sin \varphi \cos i^{(k)} - \sin \boldsymbol{\delta} \cos \varphi \sin i^{(k)} \cos a^{(k)} + \cos \boldsymbol{\delta} \cos \varphi \cos i^{(k)} \cos a^{(k)} + \cos \boldsymbol{\delta} \cos \boldsymbol{h} \sin \varphi \sin i^{(} \tag{1.9}$$

where $\varphi$ is the latitude of the location defined positive for the northern hemisphere, $\boldsymbol{h}$ is the hour angle, $i^{(k)}$ is the surface inclination defined as 0 for ceilings and $\pi/2$ for vertical walls, $a^{(k)}$ is the surface azimuth defined as $-\pi/2$ if the surface outward normal points eastward and 0 if the normal points southward, and where $\boldsymbol{\delta}$ is the solar declination.

**Shortwave radiation on a tilted surface**

The total solar irradiation $E(t, x)$ on a arbitrary surface can be determined as the sum of the direct $E_D(t, x)$, diffuse $E_d(t, x)$ and reflected $E_r(t, x)$ radiation on the surface.

$$E(t,x) = E_D(t,x) + E_d(t,x) + E_r(t,x) \tag{1.10}$$

For a known profile of direct solar irradiation on a random surface, all three factors can be determined for another arbitrary surface s. Herefore, a profile of direct solar irradiation $E_{D,\perp}(t,x)$ perpendicular on the beam radiation is retrieved from Meteonorm and used as only input parameter. The calculation of other configurations besides normal to the solar beam is performed in the model.

Different models for the determination of the diffuse radiation do exist based on an isotropic or anisotropic model of the sky dome. On account of the high importance of solar irradiation for the model[a], a more detailed determination of diffuse radiation based on a anisotropic sky dome model is favorable. Herefore, the Perez model[16;17] is implemented.

$$E_d(t,x) = A(x)E_{d,h}(t) \left[ 0.5\left(1 + \cos i\right)\left(1 - F_1\right) + F_1 \cos \xi(t,x) \cos^{-1} \xi_h(t) + F_2 \sin i \right] \tag{1.11}$$

$$E_r(t,x) = 0.5\rho A(x)\left(E_{D,h}(t) + E_{d,h}(t)\right)\left(1 - \cos i\right) \tag{1.12}$$

wherefore $A(x)$ is the surface area, $E_{d,h}$ is the diffuse horizontal radiation, $i$ is the surface inclination, $F_1$ is the circomsolar brightening coefficient, $F_2$, $\rho$ is the ground reflectance and $E_{D,h}$ is the direct horizonal radiation. The brightening coefficients $F_1$, $F_2$ are determined as

$$F_n = F_{n,1}(\varepsilon) + F_{n,2}(\varepsilon)\Delta + F_{n,3}(\varepsilon)\xi_h(t) \tag{1.13}$$

where $F_{n,i}$ are determined in the Perez model[17] based on measurements, $\varepsilon$ is the sky clearness and $\Delta$ is the sky brightness. Here, the sky brightness $\Delta$ is determined as $E_{d,h}E_{sc}^{-1}$ while the sky clearness $\varepsilon$ is determined as

$$\varepsilon = \left(E_{d,h}(t,x) + E_{D,h}(t,x)\right)E_{d,h}(t,x)^{-1} + \kappa\xi_h^3(t)\left(1 + \kappa\xi_h^3(t)\right)^{-1} \tag{1.14}$$

wherefore $E_{sc}$ is the solar constant and $\kappa$ equals 1.041.

**Solar shading**

So far, two types of structures which can shade a surface and thus reduce the shortwave radiation on a surface, i.e. an exterior screen in the pane of the surface and surface overhangs.

The implementation of an exterior solar screen in the surface pane is stratightforward. The transmitted direct solar irradiation equals $E_D(t,x)\left(1 - f_p(t)\right)$ where $f_p(t)$ is the position of the screen between 0 and 1. The total transmitted diffuse and reflected

---

[a]Solar radiation interacts e.g. with the building thermal response, heat generation by means of a thermal solar collector and power generation with a photovoltaic array

solar irradiation equals $E_d(x,t)\,(1-f_p)+f_p(t)f_s E(x,t)$ where $f_{sha}$ is the shortwave transmittance of the exterior screen.

Horizontal and vertical projectionso above and besides windows are able to intercept the direct component of solar radiation depeneding on the geometry of the obstructing and receiving surface. The usnlit area $A_{SL}(x,t)$ of a surface with width $W$ and height $H$, and vertical and horizontal projections $P_V$ and $P_H$ at a distance $R_W$ and $R_H$ of the receiving surface edges is determined as

$$A_{SL}(x,t) = [W - P_v\,|\tan\alpha(t,x)| + R_W]\left[H - P_H\tan\left(\pi - \xi_h(t)\right)\cos^{-1}\alpha(t,x) + R_H\right]$$

$$(1.15)$$

with $\alpha(t,x)$ the solar azimuth.

# Chapter 2

# Transient building response model

## 2.1 Introduction

## 2.2 Building thermal response

In this section, we describe in detail the dynamic building model and its possibilities that are implemented in Modelica as part of the IDEAS platform. The building model allows simulation of the energy demand for heating and cooling of a multi-zone building, energy flows in the building envelope and interconnection with dynamic models of thermal and electrical building energy systems within the platform for comfort measures.

The description is divided into the description of the model and the model. The window model and the model for ground losses are described more in detail as extend to the wall model.

The relevant material properties of the surfaces are complex functions of the surface temperature, angle and wavelength for each participating surface. The assumptions used frequently in engineering applications [6] are that ["each surface emits or reflects diffusely and is at a uniform temperature"] and ["the energy flux leaving a surface is evenly distributed across the surface and one-dimensional"].

### 2.2.1 Parallel opaque layers

The description of the thermal response of a or a structure of parallel opaque layers in general is structured similar to the different occurring processes, *i.e.* , the heat balance of the exterior surface, the heat balance of the interior surface and the heat conduction between both surfaces.

**Exterior surface heat balance**

The heat balance of the exterior surface $k$ is determined as

$$q_{cd}^{(k)} + q_{cv}^{(k)} + q_{sw}^{(k)} + q_{lw,e}^{(k)} = 0 \tag{2.1}$$

where $q_{cd}^{(k)}$ denotes the conductive heat flow into the wall, $q_{cv}^{(k)}$ heat transfer by convection, $q_{sw}^{(k)}$ shortwave absorption of direct and diffuse solar light, $q_{lw,e}^{(k)}$ longwave heat exchange with the environment including the sky.

*Convection.* We define the exterior convective heat flow between the exterior surfaces and the outdoor air based on an convective heat transfer coefficient as

$$q_{cv}^{(k)} = h_{cv}^{(k)} \left( T_{db,e} - T_s^{(k)} \right) \tag{2.2}$$

$$h_{cv}^{(k)} = \widetilde{\max} \left\{ 5.01 \ v_{10}^{0.85}, \ 5.6 \ ; \ 0.1 \right\} \ \text{W/m}^2\text{K} \tag{2.3}$$

where $T_{db,e}$ is the outdoor dry-bulb air temperature, $T_s^{(k)}$ is the surface temperature and $h_{cv}^{(k)}$ is the exterior convective heat transfer coefficient as defined in eqn. 2.3 where $v_{10}$ (m/s) is the wind velocity in the undisturbed flow field at 10 meter above the ground. The stated correlation with $v_{10}$ is introduced to account for buoyancy driven convection at low wind velocities and forced convection induced by increasing velocities, and is valid for a $v_{10}$ range of $[0.15, 7.5]$ m/s. [18;19]

*Longwave radiation.* We define the longwave radiative heat flow between the exterior surface and the environment as

$$q_{lw,e}^{(k)} = \sigma \varepsilon_{lw}^{(k)} \left( T_s^{(k),4} - F_{ce}^{(k)} T_{ce}^4 - (1 - F_{ce}^{(k)}) T_{db}^4 \right) \tag{2.4}$$

as derived from the Stefan-Boltzmann law wherefore $\sigma$ is the Stefan-Boltzmann constant, $\varepsilon_{lw}^{(k)}$ is the longwave emissivity of the exterior surface, $F_{ce}^{(k)}$ the radiant-interchange configuration factor between the surface and the celestial dome as defined in eqn. **??**, $T_s^{(k)}$ is the surface temperature and $T_{db}$ and $T_{ce}$ are the outdoor dry bulb and celestial dome temperature respectively. [20–23] The stated eqn. 2.4 is derived under the assumption that the ground temperature equals the outdoor air temperature, and that we can treat the surrounding outer environment as a much larger enclosure compared to the surface area.

*Shortwave radiation.* We define the absorbed shortwave solar irradiation by the exterior surface in relation to the incident irradiation as

$$q_{sw}^{(k)} = \varepsilon_{sw}^{(k)} \left( E_{Sd}^{(k)} + E_{SD}^{(k)} \right) \tag{2.5}$$

where $\varepsilon_{sw}^{(k)}$ is the shortwave absorption of the surface, and $E_{Sd}^{(k)}$ and $E_{SD}^{(k)}$ are respectively the diffuse and direct solar irradiation striking the depicted exterior surface as defined in eqns. **??**.

**Interior surface heat balance**

The heat balance of the interior surface is determined as

$$q_{cd}^{(k)} + q_{cv}^{(k)} + \sum_{j \in \mathcal{J}^{(k)}} q_{sw,j}^{(k)} + \sum_{j \in \mathcal{J}^{(k)}} q_{lw,j}^{(k)} = 0 \tag{2.6}$$

where $q_{cd}^{(k)}$ denotes the heat flow into the wall, $q_{cv}^{(k)}$ te heat transfer by convection, $q_{sw}^{(k)}$ the shortwave absorption of direct and diffuse solar light entering the interior zone through windows and $q_{lw}^{(k)}$ the longwave heat exchange with the surrounding interior surfaces.

*Convection.* We define the interior convective heat flow between the interior surfaces and zone air based on an convective heat transfer coefficient as

$$q_{cv}^{(k)} = h_{cv}^{(k)} \left( T_{db,i} - T_s^{(k)} \right) \tag{2.7}$$

$$h_{cv}^{(k)} = \widetilde{\max} \left\{ 1, \, n_1^{(k)} D^{(k) n_2^{(k)}} \left| T_{db,i} - T_s^{(k)} \right|^{n_3^{(k)}}; 0.1 \right\} \tag{2.8}$$

similar to eqn. 2.2 with $T_{db,i}$ the indoor dry-bulb temperature, $T_s^{(k)}$ the surface temperature and $h_{cv}^{(k)}$ the interior natural convective heat transfer coefficient. As the room-side heat transfer coefficient couples the room air temperature to the temperature of building components, detailed computation of its value is important. Therefore we define $h_{cv}^{(k)}$ as in eqn. 2.8 where $D^{(k)}$ is the characteristic length of the surface, $T_{db}$ is the indoor air temperature, $T_s^{(k)}$ the surface temperature and $n_x^{(k)}$ are coefficients correlating the occurring buoyancy forces and the heat transfer. These parameters $\{n_1^{(k)}, n_2^{(k)}, n_3^{(k)}\}$ are set identical to $\{1.823, -0.121, 0.293\}$ for vertical surfaces, $\{2.175, -0.076, 0.308\}$ for horizontal surfaces with enhanced convection, *i.e.* , with a heat flux in the same direction as the buoyancy force, and $\{2.72, -, 0.13\}$ for horizontal surfaces with reduced convection, *i.e.* , with a heat flux in the opposite direction as the buoyancy force as defined by Khalifa *et al.* and Awbi *et al.* [24;25] Note that the interior natural convective heat transfer coefficient is only described as function of the temperature difference. An overview of more detailed correlations including the possible higher air velocities due to mechanical ventilation can be found in literature but are not implemented. [26]

*Longwave radiation.* Longwave radiation between two internal surface $k$ and $j$ can be described by a thermal circuit formulation as [27–29]

$$q_{lw,j}^{(k)} = \sigma \left( \frac{\varsigma_{lw}^{(k)}}{\varepsilon_{lw,j}} + \frac{1}{F_j^{(k)}} + \frac{A^{(k)}}{\sum A_{j \in \mathcal{J}^{(k)}}} \right)^{-1} \left( T_s^{(k),4} - T_{s,j}^4 \right) \tag{2.9}$$

$$F_j^{(k)} = \int_{\Omega_j} \cos \theta_p \cos \theta_x \pi^{-1} S_j^{(k),-2} d\Omega_j \tag{2.10}$$

wherefore $\varepsilon_{lw}^{(k)}$ and $\varepsilon_{lw,j}$ are the longwave emissivities of the surfaces, $F_j^{(k)}$ is radiant-interchange configuration factor between these surfaces, $A^{(k)}$ and $A_j$ are the areas of surfaces $k$ and $j$ respectively wherefore $\mathcal{J}^{(k)}$ is the set of all surfaces $j$ surrounding surface $k$, $\sigma$ is the Stefan-Boltzmann constant and $T_s^{(k)}$ and $T_{s,j}$ are the respective surface temperatures. [20–23]

The above description of longwave radiation for a room or thermal zone results in the necessity of a very detailed input, *i.e.* , the configuration between all surfaces needs to be described by their shape, position and orientation in order to define $F_j^k$ as eqn. 2.10 which introduces main difficulties for windows and internal heat gain sources in the zone of interest. Simplification is achieved by means of a delta-star transformation and by definition of a (fictive) radiant star node in the zone model. [30] Literature shows that the overall model is not significantly sensitive to this assumption. [31] The heat exchange by longwave radiation between surface $s_i$ and the radiant star node in the zone model can be described as

$$\sum_{j \in \mathcal{J}^{(k)}} \boldsymbol{q}_{lw,j}^{(k)} = \sigma \left( \frac{\varsigma_{lw}^{(k)}}{\varepsilon_{lw,j}} + \frac{A^{(k)}}{\sum A_{j \in \mathcal{J}^{(k)}}} \right)^{-1} \left( \boldsymbol{T}_s^{(k),4} - \boldsymbol{T}_{rs}^4 \right) \qquad (2.11)$$

where $\varepsilon_x$ is the emissivity of surface $x$, $\varsigma_{lw}$ equals $1 - \varepsilon_x$, $A_x$ is the area of surface, $\sum_j A_x$ is the sum of areas for all surfaces $s_j$ of the thermal zone, $\sigma$ is the Stefan-Boltzmann constant [22] and $T_{si}$ and $T_{si}$ are the temperatures of surfaces $x$ and the radiant star node respectively.

*Shortwave radiation.* Absorption of shortwave solar radiation on the interior surface is handled equally as for the outside surface. Determination of the receiving solar radiation on the interior surface after passing through windows is dealt with in the zone model.

**Wall conduction process**

For the purpose of dynamic building simulation, the partial differential equation of the continuous time and space model of heat transport through a solid is most often simplified into ordinary differential equations with a finite number of parameters representing only one-dimensional heat transport through a construction layer. Within this context, the wall is modeled with lumped elements, i.e. a model where temperatures and heat fluxes are determined from a system composed of a sequence of discrete resistances and capacitances $R_{n+1}$, $C_n$. The number of capacitive elements $n$ used in modeling the transient thermal response of the denotes the order of the lumped capacitance model.

$$\boldsymbol{Q}_{\text{net},x} = \frac{\partial \boldsymbol{T}_{ci}}{\partial t} C_x = \sum_i^n \boldsymbol{Q}_{\text{res},x} + \boldsymbol{Q}_{\text{source},x} \qquad (2.12)$$

where $\dot{Q}_{\text{net},x}$ is the added energy to the lumped capacity, $T_{ci}$ is the temperature of the lumped capacity, $C_{ci}$ is the thermal capacity of the lumped capacity equal to $\rho_x c_x d_c A_x$

for which $\rho_x$ denotes the density and $c_x$ is the specific heat capacity of the material and $d_{\text{ci}}$ the equivalent thickness of the lumped element, where $\dot{Q}_{\text{res},x}$ the heat flux through the lumped resistance and $R_{\text{ri}}$ is the total thermal resistance of the lumped resistance equal to $d_{\text{ri}}\left(\lambda_x A_x\right)^{-1}$ for which $d_{\text{ri}}$ denotes the equivalent thickness of the lumped element and where $\dot{Q}_{\text{source}}$ are internal thermal source, *e.g.* from embedded systems.

## 2.2.2 Windows

The thermal model of a is similar to the model of an exterior wall but includes the absorption of solar irradiation by the different glass panes, the presence of gas gaps between different glass panes and the transmission of solar irradiation to the adjacent indoor zone.

*Gap heat transfer.* The total convective and longwave heat transfer through thin gas gaps as present in modern glazing systems is described as

$$q_{cd} = \mathbf{Nu}_g \frac{\lambda_g}{d_g}\left(\boldsymbol{T}_s^{(k)} - \boldsymbol{T}_s^{(j)}\right) + \sigma \frac{\varepsilon_k \varepsilon_j}{1 - \varsigma_k \varsigma_j}\left(\boldsymbol{T}_{s,k}^4 - \boldsymbol{T}_{s,j}^4\right) \tag{2.13}$$

$$\mathbf{Nu}_g = n_{\text{i},1} \mathbf{Gr}_g^{n_{\text{i},2}} \tag{2.14}$$

$$\mathbf{Gr}_g = g\beta\rho^2 d_g^3 \mu^{-2}\left(\boldsymbol{T}_{\text{si}} - \boldsymbol{T}_{\text{sj}}\right) \tag{2.15}$$

where $A_x$ is the glazing surface, $d_x$ is the gap width, $\text{Nu}_x$ is the Nusselt number of the gas, $\varepsilon_x$ is the longwave emissivity of the surfaces, $\varsigma_x$ equals $1 - \varepsilon_x$ and $T_{\text{si}}$ is the surface temperature. The Nusselt number of the present gas in the gap describing the ratio of convective to conductive heat transfer is generally described is where $\text{Gr}_x$ is the Grashof number approximating the ratio of buoyancy to viscous force acting on the window gap gas, $g$ is the gravitational acceleration, $\beta$ is the coefficient of thermal expansion, $\rho$ is the gas density, $\mu$ is the gas viscosity and $n_{\text{i},:}$ are correlation coefficients. These parameters $\{n_{\text{i},1}, n_{\text{i},2}\}$ are identical to $\{1.0, 0\}$ for all $\text{Gr}_x$ below $7.10^3$, $\{0.0384, 0.37\}$ for all $\text{Gr}_x$ between $10^4$ and $8.10^4$, $\{0.41, 0.16\}$ for all $\text{Gr}_x$ between $8.10^4$ and $2.10^5$ and $\{0.0317, 0.37\}$ for all $\text{Gr}_x$ above $2.10^5$.

*Shortwave optical properties.* The properties for absorption by and transmission through the glazing are taken into account depending on the angle of incidence of solar irradiation and are based on the output of the WINDOW 4.0 software[32][?] as validated by Arasteh[33] and Furler[34]. Within this software, the angular dependence of the optical properties is determined based on the model of Furler[35]. The reflectivity $r$ and transmissivity $t$ are determined with the Fresnel equations[36] and Snell's Law of refraction[37], based on the relative refractive index n as follows

$$r_x = 0.5\sin^2\Delta_x \sin^{-2}\Delta_x + 0.5\tan^2\Delta_x \tan^{-2}\Delta_x \tag{2.16}$$

$$\Delta_x = \xi_x - \xi_x' \text{ st. } \sin\xi_x = n\sin\xi_x' \tag{2.17}$$

where $\Delta_x = \xi_x - \xi_x'$ wherefore counts that $\sin\xi_x = n\sin\xi_x'$. The resulting transmittance $T_x$ and reflectance $R_x$ for a single glass pane after multiple reflections is

obtained from

$$T_x = t_0^2 \exp\left(-\alpha_x d_x / \cos\xi_x\right) \left(1 - r_x^2 \exp\left(-\alpha d_x / \cos\xi_x\right)\right)^{-1} \tag{2.18}$$

$$R_x = r_x \left(1 + T_x \exp\left(-\alpha_x d_x / \cos\xi_x\right)\right) \tag{2.19}$$

where $d_x$ is the thickness of the pane and $\alpha_x$ is absorption coefficient. The total transmittance $T_x$ and the absorptances $A_{i,:}$ for multipane windows are retrieved using iterative equations taking into account the multiple internal reflections within the glazing system.

The resulting output from WINDOW 4.0 [?] depicts an array of the transmittances $T$ through the window and the absorptances $A_x$ for each glass pane $x$ for $\xi_x \in \{(k/18)\}$ with $k \in \{0, 1, \ldots, 9\}$. The same array input is used in other dynamic building simulation tools, e.g. in TRNSYS[?] where values for different angles are retrieved by means of linear interpolation.

## 2.2.3 Ground slabs

The heat flow through building envelope constructions in contact with a is the same for the interior surface and the conduction process, but differs at the exterior surface in contact with the ground. As the heat transfer through the ground is 3-dimensional and defined by a large time lag, the exterior surface heat balance is generally approximated based on ISO 13370.

The total heat flow through the ground is given by

$$\dot{Q}_{\mathrm{net},i} = L_{\mathrm{S},i} \left[\bar{T}_i - \bar{T}_e\right] - L_{\mathrm{pi},i}\hat{T}_i \cos\gamma_i + L_{\mathrm{pe},i}(x)\hat{T}_e \cos\gamma_e \tag{2.20}$$

where $L_{\mathrm{S},i}$ is the steady-state thermal coupling coefficient, $L_{\mathrm{pi}}$ and $L_{\mathrm{pe}}$ are the internal and external periodic thermal coupling coefficients respectively, $\bar{T}$ is the annual average temperature, $\hat{T}$ is the annual average temperature amplitude, and $\gamma_i$ and $\gamma_e$ determine the time lag of the heat flow cycle compared with that of the internal and external temperature respectively.

The steady-state and periodic thermal coupling coefficient area is determined as

$$L_{\mathrm{S},i} = A_x \frac{\lambda_g}{0.457 B_t + d_t + 0.5z} + zP \frac{2\lambda_g}{\pi z} \left[1 + \frac{0.5d_t}{d_t + z}\right] \ln\left[\frac{z}{d_{\mathrm{t},i}} + 1\right] \tag{2.21}$$

$$L_{\mathrm{pi},i} = A_x \frac{\lambda_{\mathrm{g}}}{d_{\mathrm{t},i}} \sqrt{\frac{2}{\left[1 + \frac{\delta}{d_{\mathrm{t},i}}\right]^2 + 1}} \quad \text{and} \quad L_{\mathrm{pe},i} = 0.37 P_x \lambda_{\mathrm{g}} \ln\left[\frac{\delta}{d_{\mathrm{t},i}} + 1\right] \tag{2.22}$$

where $A_x$ is the wall area, $\lambda_{\mathrm{g}}$ is the thermal conductivity of the unfrozen ground, $B_{\mathrm{t},i}(x)$ is the characteristic dimension of the floor, $d_{\mathrm{t},i}$ is the equivalent thickness of the wall construction, $z$ is the depth of the wall (i.e. floor) below ground level, $\delta$ is

periodic penetration depth (i.e. the depth in the ground at which the temperature amplitude is reduced to $e^{-1}$ of that at the surface) and $P_x$ is the exposed perimeter of the wall. The angle $\gamma_e$ is determined as $2\pi t/t_{yr} + \pi/12 - \arctan d_{t,i}/(d_{t,i} + \delta)$ and $\gamma_e$ is determined as $2\pi t/t_{yr} + \pi/12 + 0.22 \arctan \delta/(d_{t,i} + 1)$.

## 2.2.4 Zones

Consisting of both the convective as radiative calculation for determination of thermal comfort.

**Thermal response model**

Also the thermal response of a can be divided into a convective, longwave radiative and shortwave radiative process influencing both thermal comfort in the depicted zone as well as the response of adjacent wall structures.

The air within the zone is modeled based on the assumption that it is well-stirred, i.e. it is characterized by a single uniform air temperature. This is practically accomplished with the mixing caused by the air distribution system. The convective gains and the resulting change in air temperature $T_a$ of a single thermal zone can be modeled as a thermal circuit. The resulting heat balance for the air node can be described as

$$\frac{\partial T_a}{\partial t} c_a V_a = \sum_i^N \dot{Q}_{i,a} + \sum_i^{n_s} R_{ci}^{-1} A_x [T_a - T_{si}] + \sum_i^{n_z} \dot{m}_{a,z} [h_a - h_{a,z}]$$
$$+ \dot{m}_{a,e} [h_a - h_{a,e}] + \dot{m}_{a,sys} [h_a - h_{a,sys}]$$

(2.23)

wherefore the specific air enthalpy $h_a$ is determined as $c_a \vartheta_a + \chi_a c_w \vartheta_a + \chi_a h_{w,ev}$ and where $T_a$ is the air temperature of the zone, $c_a$ is the specific heat capacity of air at constant pressure, $V_a$ is the zone air volume, $\dot{Q}_a$ is a convective internal load, $R_{ci}$ is the convective surface resistance of surface $x$, $A_x$ is the area of surface $x$, $T_{si}$ the surface temperature of surface $x$, $\dot{m}_{a,z}$ is the mass flow rate between zones, $\dot{m}_{a,e}$ is the mass flow rate between the exterior by natural infiltration, $\dot{m}_{a,sys}$ is the mass flow rate provided by the ventilation system, $\vartheta_a$ is the air temperature in degrees Celsius, $\chi_a$ is the air humidity ratio, $c_w$ is specific heat of water vapor at constant pressure and $h_{w,ev}$ is evaporation heat of water at 0 degrees Celsius.

Infiltration and ventilation systems provide air to the zones, undesirably or to meet heating or cooling loads. The thermal energy provided to the zone by this air change rate can be formulated from the difference between the supply air enthalpy and the enthalpy of the air leaving the zone $h_a$. It is assumed that the zone supply air mass flow rate is exactly equal to the sum of the air flow rates leaving the zone, and all air streams exit the zone at the zone mean air temperature. The moisture dependence of the air enthalpy is neglected in most cases.

A multiplier for the zone capacitance $f_{c,a}$ is included. A $f_{c,a}$ equaling unity represents just the capacitance of the air volume in the specified zone. This multiplier can be

greater than unity if the zone air capacitance needs to be increased for stability of the simulation. This multiplier increases the capacitance of the air volume by increasing the zone volume and can be done for numerical reasons or to account for the additional capacitances in the zone to see the effect on the dynamics of the simulation. This multiplier is constant throughout the simulation and is set to 5.0 if the value is not defined.

The exchange of longwave radiation in a zone has been previously described in Sect. 2.2.1.2 by Eq. 2.6 and further considering the heat balance of the interior surface. Here, an expression based on *radiant interchange configuration factors* of *view factors* is avoided based on a delta-star transformation and by definition of a *radiant star temperature* $T_{rs}$. Literature[31] shows that the overall model is not significantly sensitive to this assumption. This $T_{rs}$ can be derived from the law of energy conservation in the radiant star node as $\sum_i Q_{i\text{-}rs}$ must equal zero. Long wave radiation from internal sources are dealt with by including them in the heat balance of the radiant star node resulting in a diffuse distribution of the radiative source.

Transmitted shortwave solar radiation is distributed over all surfaces in the zone in a prescribed scale. This scale is an input value which may be dependent on the shape of the zone and the location of the windows, but literature[31] shows that the overall model is not significantly sensitive to this assumption.

# Chapter 3

# THERMAL BUILDING SYSTEM

## 3.1 Introduction

The library is based on Modelica.Thermal.FluidHeatFlow and not on Modelica.Fluid or Modelica.Media. This makes the library easier to compile by a variety of tools that might not (yet) fully support the Modelica.Fluid and Modelica.Media libraries.

## 3.2 Hydraulic components

### 3.2.1 Basic components for Joe the plumber

1. pipe
2. pump
3. ambient
4. three-way valve
5. pressure grounding

### 3.2.2 Thermal energy storage tank

**Buffer tank**

*IDEAS.Thermal.Components.Storage.StorageTank*

Buffer tank (no internal heat exchangers) composed of an array of interconnected pipes. Except for the internal heat exchanger, this model is identical to IDEAS.Thermal.Components.Storage.StorageTankOneIntHX. Therefore, the model description can be found in

The following phenomena are modelled:

1. thermal stratification due to discretization in layers (1D)
2. energy and mass balance on layer level
3. conductive heat losses to the environment base on tank geometry
4. thermal conduction through the water between the layers
5. buoyancy in case of temperature inversion

with ambient heat losses (= nodes or layers). The number of nodes $nbrNodes$ is a parameter and an array of $nbrNodes + 1$ $FlowPort$ connectors is available to connect to each intersection between the layers.

**Tank with internal heat exchanger**

This tank is similar to $IDEAS.Thermal.Components.Storage.StorageTank$ except that an internal heat exchanger is added. The heat exchanger can be positioned in any continuous section of layers, it is modelled with one heat exhanger node per tank node.

$$mc_p \frac{dT_i}{dt} = \dot{m}_i c_p (T_{i-1} - T_i) + \dot{q}_i \tag{3.1}$$

In this equation, $\dot{q}_i$ is composed of different heat transfer phenomena:

$$\dot{q}_i = \dot{q}_{conduction,\ i-1} - \dot{q}_{conduction,\ i} + \dot{q}_{loss,\ i} + \dot{q}_{buoyancy,\ i} \tag{3.2}$$

$$\dot{q}_{conduction,\ i} = \frac{\lambda_{water} S}{h_{node}} (T_{i-1} - T_i) \tag{3.3}$$

$$\dot{q}_{loss,\ i} = U A_{loss} (T_i - T_{ambient}) \tag{3.4}$$

$$\dot{q}_{buoyancy,\ i} = \text{ if } (T_{i-1} \geq T_i \geq T_{i+1}) \text{ then } 0 \text{ else } ??? \tag{3.5}$$

A first attempt was to suppose that buoyancy can be modelled with an equivalent thermal conductivity.

$$\text{if } (T_i \leq T_{i+1}) \text{ then } \dot{q}_{buoyancy} = \lambda_{buoyancy} S (T_{i+1} - T_i) \tag{3.6}$$

To find $\lambda_{buoyancy}$, an optimization is carried out in which for different number of nodes, the $\lambda_{buoyancy}$ that assures the best fit of the end temperatures for both charging experiments is found.

The results show that for a given number of nodes, this leads to acceptable validation results for the charging experiment. However, the equivalent thermal conductivity is strongly dependent on the number of nodes. As this can be due to the variable node height, mass and DT between the nodes, a model with a parameter that clearly depends on the number of nodes is not useful for sensitivity studies in which for example the tank volume and geometry is changed.

A second approach is to suppose that buoyancy is actually a mass flow rate phenomena, caused by different densities of the water as a function of temperature. Therefore, the following equation is used as a starting point.

$$\text{if } (T_i \leq T_{i+1}) \text{ then } \dot{q}_{buoyancy} = \dot{m}_{buo} c_p (T_{i+1} - T_i) \tag{3.7}$$

We suppose $\dot{m}_{buo}$ depends on the temperature gradient, and is zero when the temperature difference between the layers is zero.

$$\dot{m}_{buo} = k_{buo} \left(\frac{dT}{dh}\right)^{\exp_{buo}} \tag{3.8}$$

Again, optimization is used in order to identify $k_{buo}$ and $\exp_{buo}$ as a function of the number of nodes. Again, we see that these coefficients are depending on the number of nodes. We also see that the sensitivities on the obtained end temperatures in the charging experiment is large.

## 3.2.3 Heat production

**Partial heater**

All hydraulic heater models extend from this partial heater model. tbc

**Boiler**

**Heat pumps**

1. modulating air-source hp
2. ground-source hp
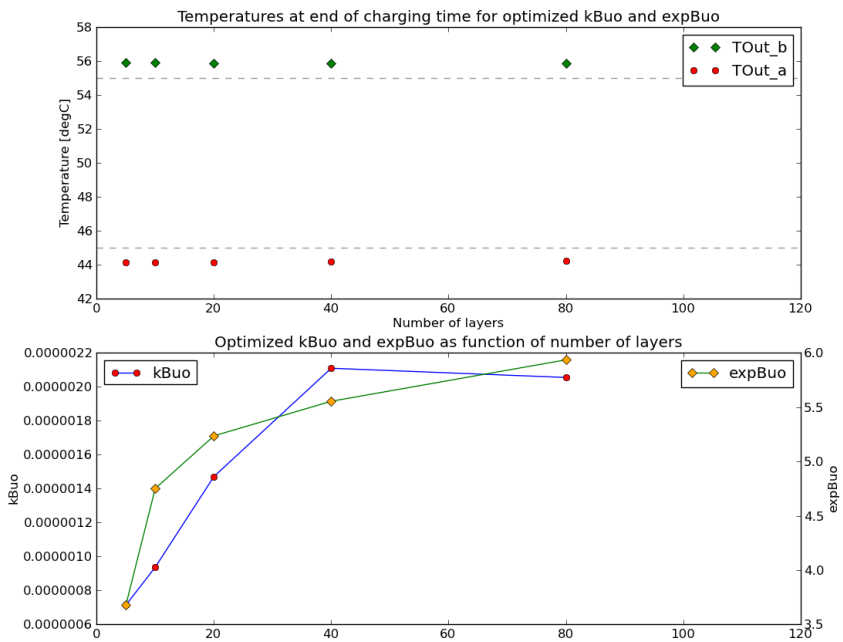
**Figure 3.1:** Result of the non-linear parameter fitting
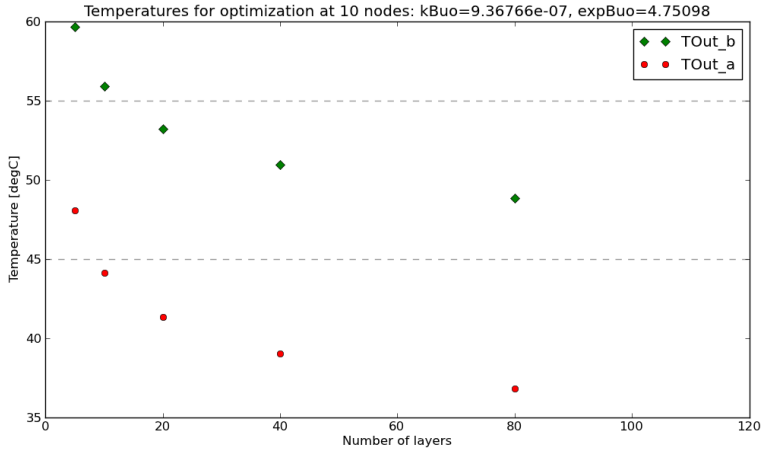
**Figure 3.2:** Resulting temperatures when the found values for 10 nodes are used

## 3.2.4 Heat emission

**Partial heat emission model**

**Radiator**

**Embedded pipe for thermally activated building systems (TABS)**

From [38]

## 3.3 **Heating systems**

## 3.3.1 Ideal heating

**Hydraulic heating**

Main hydraulic scheme with replaceable models for heat production, heat emission, solar thermal system and control.

3.3.2 Solar thermal system

3.3.3 Domestic hot water production

3.4 **Vertical ground heat exchanger**

3.4.1 Model Harm Leenders

3.4.2 Model Dieter Patteeuw

3.5 **Control**

# Chapter 4

# Electricity system

In this section, we describe in detail the electrical models that are implemented in Modelica as part of the IDEAS platform. These are models on the production, electrical distribution and storage side. First the photovoltaic (PV) system is treated which produces electricity locally from solar energy. In a second part, the distribution of electricity on distribution level is described.

Work in progress are the in-home electricity grid and the electrical storage in batteries.

## 4.1 Photovoltaic system

First, a photovoltaic (PV) system is implemented based on the five parameter model to simulate the energy production from a photovoltaic system under operational conditions. The five parameter model, which is temperature dependent, is based on the single diode equivalent circuit of a PV panel [39;40]. The five parameters are:

- the light current, $I_{ph}$;
- the diode reverse saturation current, $I_o$;
- a shunt resistance, $R_{sh}$;
- a series resistance, $R_s$;
- the thermal voltage, $V_t$.

These parameters are indicated in the equivalent circuit presented in Figure **??**.

### 4.1.1 Power output of PV panel

The electrical output from a PV system depends on the solar radiation, the ambient temperature of the cells, the solar incidence angle and the load. The solar radiation,
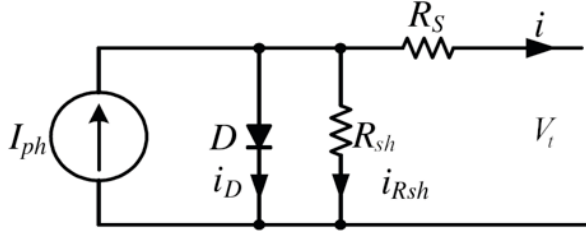
**Figure 4.1:** Five parameter model of a PV panel[39]

incidence angle and temperature is obtained from chapter **??**. The parameters needed for the model can generally be obtained from data gathered from the manufacturer's specifications of the solar panels. The required specifications to calculate the five parameters are the current $I_{mpp}$ and voltage $V_{mpp}$ at maximum power point (mpp) under standard testing conditions (STC)[a], the short circuit current $I_{sc}$ and open circuit voltage $V_{oc}$ under the same standard testing conditions, the temperature coefficients $k_i$ and $k_v$ of respectively the short circuit current and open circuit voltage and the nominal cell temperature under STC $T_{c,ref}$.

The general current-voltage $(i-v)$ equation for the single diode equivalent circuit is given in Eq. (4.1). This equation can be written for three points: $(i)$ short-circuit, $(ii)$ open-circuit and $(iii)$ maximum power point[40].

$$i(t) = I_{ph} - I_0 \left( e^{\frac{v(t)+i(t)R_s}{n_s V_t}} - 1 \right) - \frac{v(t) + i(t)R_s}{R_{sh}} \tag{4.1}$$

In this equation $V_t$ is the junction thermal voltage and $n_s$ the number of cells in the panel connected in series:

$$V_t = \frac{f_A k T_{stc}}{q} \tag{4.2}$$

with $f_A$ the ideality factor, $k$ the Boltzmann's constant $(1.380663 \cdot 10^{-23}$ J/K), $q$ the charge of an electron $(1.600218 \cdot 10^{-19}$ C) and $T_{stc}$ the cell temperature under STC.

The voltage $V_{mpp}$ and current $I_{mpp}$ at maximum power point should satisfy Eq. (4.1). The derivative of the power with respect to the voltage $(dP/dV)$ at $V_{mpp}$ and $I_{mpp}$ should be zero Eq. (4.3). The derivative of the current with respect to the voltage $(dI/dV)$ at short circuit current should be the negative of the shunt conductance $(R_{sh}^{-1})$. These equations lead to the calculation of the parameters $R_s$, $R_{sh}$ and $V_t$.

The maximum power point $P_{mpp}$ (at $I = I_{mpp}$) can be found with Eq. (4.3):

$$\frac{dP}{dV} = I_{mpp} + V_{mpp} \frac{-\frac{(I_{sc}R_{sh}-V_{oc}+I_{sc}R_s)e^{\frac{V_{mpp}+I_{mpp}R_s-V_{oc}}{n_s V_t}}}{n_s V_t R_{sh}} - \frac{1}{R_{sh}}}{1 + \frac{(I_{sc}R_{sh}-V_{oc}+I_{sc}R_s)e^{\frac{V_{mpp}+I_{mpp}R_s-V_{oc}}{n_s V_t}}}{n_s V_t R_{sh}} + \frac{R_s}{R_{sh}}} \tag{4.3}$$

[a]Standard testing conditions are $(i)$ an irradiance of 1000 W/m$^2$ and $(ii)$ a cell temperature of 25°C and $(iii)$ reference air mass of 1.5

The reverse saturation current $I_o$ and light current $I_{ph}$ at STC can be found based on Eq. (4.1) for the short circuit (Eq. (4.4)) and open circuit condition (Eq. (4.5)).

$$I_{sc} = I_{ph} - I_0 e^{\frac{I_{sc}R_s}{n_s V_t}} - \frac{I_{sc}R_s}{R_{sh}} \tag{4.4}$$

$$I_{oc} = 0 = I_{ph} - I_0 e^{\frac{V_{oc}}{n_s V_t}} - \frac{V_{oc}}{R_{sh}} \tag{4.5}$$

The PV parameters are adjusted to take into account the position of the sun, the direct and indirect radiation and the ambient temperature. The cell temperature has been adjusted to be the ambient temperature plus the losses of the panel. The parameters for the non-reference conditions are calculated in the next paragraphs.

The tilt angle and orientation of the PV panels are parameters of the PV model. Together with the sun's position, the incidence angle of the direct beam radiation can be calculated which allows to obtain the amount of radiation that gets reflected by and passes through the PV panel cover. This is done using incidence angle modifiers that are derived from De Soto et al.[39]. The incidence angle modifier $K_{\tau\alpha}(\theta)$ can be found from the transmittance $\tau$ of the cover system with Eq. (4.8), which is approximated in Eq. (4.7). The angle of refraction, $\theta_r$, is determined in Eq. (4.6) by Snell's law, with $\theta$ the incidence angle and $n$ the effective index of refraction of the cell cover. In Eq. (4.7), $f_K$ is the glazing extinction coefficient and $f_L$ is the glazing thickness. In the model $f_K$ and $f_L$ can be adjusted. By default, $f_K$ is assumed to be 4 $m^{-1}$ and $f_L$ is assumed to be 2 $mm$.

$$\theta_r = \arcsin(n \sin\theta) \tag{4.6}$$

$$\tau(\theta) = e^{-\frac{f_K f_L}{\cos\theta_r}} \left[ 1 - \frac{1}{2} \left( \frac{\sin^2(\theta_r - \theta)}{\sin^2(\theta_r + \theta)} + \frac{\tan^2(\theta_r - \theta)}{\tan^2(\theta_r + \theta)} \right) \right] \tag{4.7}$$

$$K_{\tau\alpha}(\theta) = \frac{\tau(\theta)}{\tau(0)} \tag{4.8}$$

The incidence angle modifiers and the direct and diffuse radiation, which are inputs to the model, allow together with the reflected radiation to calculate the absorbed solar radiation $S$ in Eq. (4.9). In this equation $G_b$ is the direct, $G_d$ the diffuse and $G$ the total radiation. The slope of the PV panel is characterized by $\beta$.

$$\frac{S}{S_{ref}} = \frac{G_b}{G_{ref}} K_{\tau\alpha,b} + \frac{G_d}{G_{ref}} K_{\tau\alpha,d} \frac{1 + \cos\beta}{2} + \frac{G}{G_{ref}} \rho K_{\tau\alpha,g} \frac{1 - \cos\beta}{2} \tag{4.9}$$

with

$$S_{ref} = G_{ref} e^{-f_K f_L} \tag{4.10}$$

and $G_{ref}$ is the irradiance at STC (1000 W/m$^2$).

The light current $I_{ph}$, reverse saturation current $I_0$ and thermal voltage $V_t$ at non-reference conditions can be calculated when the temperature, open circuit voltage and short circuit current are known [40]. The open circuit voltage $V_{oc}$ can be calculated using Eqns. (4.11) and (4.12). The short circuit current $I_{sc}$ can be found using Eq. (4.13).

$$e^{\frac{V_{oc}(S)}{n_s V_t}} = \frac{I_{ph}(S)R_{sh} - V_{oc}(S)}{I_0 R_{sh}} \tag{4.11}$$

$$V_{oc}(T) = V_{oc} + k_v(T - T_{stc}) \tag{4.12}$$

$$I_{sc}(S,T) = I_{sc}\left(\frac{S}{S_{ref}}\right)\left(1 + \frac{k_i}{100}(T - T_{ref})\right) \tag{4.13}$$

The reverse saturation current $I_0$ can be calculated with Eq. (4.14). The light current $I_{ph}$ is found using Eq. (4.15).

$$I_0 = \left(I_{sc} - \frac{V_{oc} - I_{sc}R_s}{R_{sh}}\right)e^{-\frac{V_{oc}}{n_s V_t}} \tag{4.14}$$

$$I_{ph} = I_0 e^{\frac{V_{oc}}{n_s V_t}} + \frac{V_{oc}}{R_{sh}} \tag{4.15}$$

## 4.1.2 Power output of PV system

A PV system consists of multiple PV panels connected in series. Assuming that all PV panels are in the same condition, the output DC voltage can be multiplied by the number of PV panels in a PV system.

The number of PV panels is a parameter of the general PV system model. The peak power $P_{peak}$ is defined with $V_{mpp}$, $I_{mpp}$ and the number of panels $n_p$:

$$P_{peak} = n_p V_{mpp} I_{mpp} \tag{4.16}$$

## 4.1.3 Orientation PV system

The PV system has two orientation parameters, namely (*i*) the azimuth and (*ii*) the inclination angle. An azimuth angle of 0° is defined as towards the South, -90° for the East and 90° for the West. Applied to Belgium, the PV system has the highest annual electricity production when the system is oriented directly to the South with an inclination of 34°.

The inclination and azimuth angles are paremeters of the modeled photovoltaic system.

### 4.1.4 Inverter

A PV system is connected to the electrical grid through an inverter, which converts the generated DC power to AC power with an efficiency $\eta_{dc/ac}$.

Due to the lack of simultaneity of production and consumption, a bidirectional energy flow may occur between a building and the electrical grid (e.g. low voltage grid for residential buildings), which may lead to voltage instabilities on the grid (e.g. increasing voltages due to the injection of electricity, unbalance, etc.). To avoid excessive feeder voltages at the moments of re-injecting PV power in the grid, the inverter is curtailed when a predefined voltage limit is reached. Curtailing of a PV system means production losses.

## 4.2 **Electrical distribution grid**

In the electrical grid system two types of grids exist, namely (*i*) distribution and (*ii*) transmission grids[41;42]. However, in Belgium, distribution grids differ fundamentally from transmission grids:

- They are mostly radially: This means there is only one feeding transformer[b]. Due to the lack of a redundant supply, the reduced reliability is a major disadvantage. In case of a fault, all loads behind the fault will be switched off.

- The lower the voltage level, the higher the R/X ratio. Thus, low voltage residential distribution grids are highly resistive.

An electrical distribution grid for low voltage is modeled. E.g. a residential district is typically a radial distribution grid with a rated nominal voltage of 230/400 V[c] wye (or star) connection. Both a single-phase en three-phase grid can be simulated. The single-phase grid can serve for fully balanced simulations.

First, the grid topology is described. As will be shown, any radial grid can be easily represented by two matrices, namely the incidence and impedance matrix. Second, the background for the power flow analysis will be described to determine the nodal currents, line currents and nodal voltages. Radial grids are, compared to meshed grids, more easy to analyze and because of the low cost, it is prefered for distribution grids[41]. Figure 4.2 gives an example of a radial grid. This figure shows an IEEE 34 node test feeder[43].

### 4.2.1 Grid topology

Distribution grids for low-voltage are mostly radial grids. In this case, a residential three-phase distribution grid is modeled. A residential district is typically a radial

---

[b]Traditionally, there is only a unidirectional power flow.
[c]230 V phase voltage, 400 V line voltage.
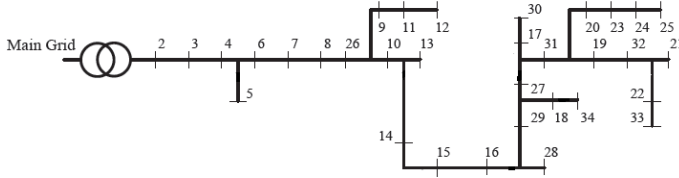
**Figure 4.2:** Grid topology IEEE 34 node test feeder [43]

feeder with a rated nominal voltage of 230/400V wye (or star) connection. For distribution grids without distributed generation (uni-directional power flow), the voltage at the feeder typically has a higher value to ensure that the voltage in the whole feeder stays within the preset boundaries. For a fully balanced system, the single-phase equivalent grid can be used. Connections to loads (e.g. buildings) are represented by nodes. Loads and generation units can be single or three-phase connected to the grid.

Any radial grid can be represented by an incidence matrix (or connection matrix) **T**. The columns correspond with the number of nodes. Each line in **T** represents a segment of the grid (branch) between two nodes. Each segment is represented by 1 and -1 at respectively the start and end node of that segment. The other row elements are zero. A node can be the start or end node of more than one segment. Since there are $n$ nodes, a radial grid consists of $n-1$ line segments. To attain a square matrix, an additional (first) row is introduced to represent the imaginary line segment between the transformer and the first node. This line segment only has an end node.

Eq. (4.17) gives an example of the representation of an incidence matrix **T** in which the nodes are all next to each other, which means branches are between consecutive nodes.

$$
\mathbf{T} = \begin{bmatrix}
-1 & 0 & 0 & \cdots & 0 & 0 & 0 \\
1 & -1 & 0 & \cdots & 0 & 0 & 0 \\
0 & 1 & -1 & \cdots & 0 & 0 & 0 \\
\vdots & \vdots & \vdots & \ddots & \vdots & \vdots & \vdots \\
0 & 0 & 0 & \cdots & -1 & 0 & 0 \\
0 & 0 & 0 & \cdots & 1 & -1 & 0 \\
0 & 0 & 0 & \cdots & 0 & 1 & -1
\end{bmatrix}
\tag{4.17}
$$

Cables, with a length $f_L$ (m), for the line segments of an electrical grid are characterized by an impedance $Z = R + jX$, with $R$ the resistance and $X$ the reactance of the cable:

$$
R = f_L r
\tag{4.18}
$$

$$
X = f_L x
\tag{4.19}
$$

with $r$ the characteristic resistance $x$ the characteristic reactance in $\Omega/m$. This allows to represent the grid with an impedance matrix $\mathbf{Z} = \mathbf{R} + j\mathbf{X}$.

In a similar way, the houseconnectors are described. These are the connection lines between the in-home grid and the grid connection node of the building. The houseconnectors are characterized by a cable type, cable length and the type of connection with the grid (single-phase or three-phase connection).

## 4.2.2 Power flow analysis

A power flow analysis is required to characterize the impact of a load profile on each connection node in the grid. A power flow analysis is performed to determine the nodal currents $\mathbf{I}_{node}$, line currents $\mathbf{I}_{line}$ and nodal voltages $\mathbf{V}_{node}$. The calculations are based on the Laws of Kirchhoff:

**Conservation of electric charge** At any node, the sum of currents flowing into the node is equal to the sum of currents flowing out of the node (Eq. (4.20)).

**Conservation of energy** The sum of the voltage drops around any closed circuit is zero (Eq. (4.21)).

$$\sum_{k=1}^{nodes} i_k(t) = 0 \tag{4.20}$$

$$\sum_{k=1}^{branches} \Delta v_k(t) = 0 \tag{4.21}$$

The voltage drop in a branch $k$ between nodes $n$ and $n+1$ is defined as:

$$\Delta v_k(t) = Z_k i_{line,k}(t) = v_n(t) - v_{n+1}(t). \tag{4.22}$$

When the nodal currents $\mathbf{I}_{node}$, line currents $\mathbf{I}_{line}$ and nodal voltages $\mathbf{V}_{node}$ are known, the total flow of apparent power $S$ can be calculated. $S$ consists of active power $P$ and reactive power $Q$:

$$S(t) = \sum_{f=1}^{phases} P_f(t) + jQ_f(t) \tag{4.23}$$

The apparent power S is calculated as:

$$S = U_{phase}I^* \tag{4.24}$$

with $U_{phase}$ the phase voltage and $I^*$ the complex conjugate of $I$.

The ohmic losses in a single-phase grid are calculated as follows:

$$P_{grid\ loss,\ 1-phase} = \sum_{k=1}^{branches} P_{k,\ loss} = \sum_{k=1}^{branches} R_k I_{k,\ line}^2 \tag{4.25}$$

A three-phase distribution grid consists of three phases and a neutral cable. Therefore, Eq. (4.25) can be rewritten for three-phase distribution grids as follows:

$$P_{grid\ loss,\ 3-phase} = \sum_{f=1}^{phases} P_{grid\ loss,\ f} + P_{neutral,\ loss} \tag{4.26}$$

## 4.2.3 Single/three-phase grid simulation

Electrical loads, generation units, storage units (e.g. batteries) can be single-phase or three-phase connected to the grid. Generally the system is not fully balanced (e.g. the same load in each phase for each node in the distribution grid) and an unbalanced three-phase power flow analysis is performed. In case of a fully balanced system, the power flow analysis can be performed on a simplified single-phase grid. For three-phase power flows, the distribution grid is represented by three phase conductors and a neutral conductor. Nodal phase voltages are the voltages with respect to the nodal voltage in the neutral conductor.

## 4.2.4 Transformer

A radial distribution grid has one feeding transformer. The low-voltage (LV) side of the transformer is connected to the distribution grid, while the high-voltage (HV) side is connected to the higher-voltage grid.

A transformator (single or three-phase) is represented by the equivalent scheme as shown in Figure 4.3. The transformer is represented by series ($Z_{s,HV}$ and $Z_{s,LV}$) and parallel element ($Z_{par}$). The series impedances represent the ohmic resistance and reactance (inductance) of respectively the high-voltage and low-voltage windings of the transformer. The parallel impedance represents the magnetic losses (or iron losses) in the core of the transformer. To define the active losses of the transformer, only the resistances of all impedances are taken into account.

The parallel element ($Z_{par}$) is defined during a no-load test of the transformer. At the primary side, the nominal voltage is applied, while the secondary windings are open. The series elements can be neglected:

$$Z_{par} = \left[ \frac{400}{\sqrt{3}} \right]^2 \left[ \frac{P_0}{3} \right]^{-1} \tag{4.27}$$

with $P_0$ the no-load losses.
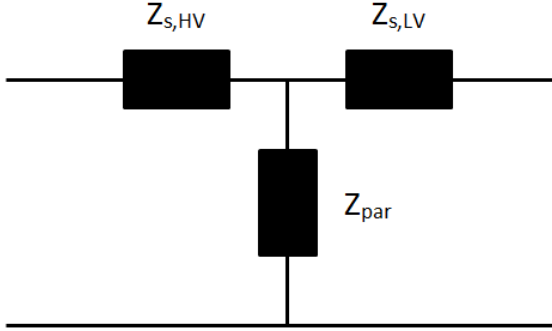
**Figure 4.3:** Equivalent scheme of a transformator

The series elements ($Z_{s,HV}$ and $Z_{s,LV}$) are defined during short-circuit tests of the transformer. During this test, the secondary windings are shorted. Since the parallel elements are large compared to the series elements, the series elements ($Z_s = Z_{s,HV} + Z_{s,LV}$) can be defined:

$$Z_s = \left[\frac{400u_k}{100\sqrt{3}}\right]^2 \left[\frac{S_n u_k}{300}\right]^{-1} \tag{4.28}$$

with $S_n$ the nominal apparent power of the transformer and $u_k$ the percentage of the short-circuit voltage[d]. Generally, $Z_s$ is evenly distributed amongst $Z_{s,HV}$ and $Z_{s,LV}$.

The active losses in a transformer are calculated as is done in Eq. (4.25) for the losses in the grid.

## 4.3 Electrical in-home grid

In progress.

## 4.4 Electrical storage

In progress.

---

[d]The short-circuit voltage is the voltage that has to be applied at the primary winding to have the nominal current in the primary winding when the secondary winding is shorted.

# II

# Validation or verification

# III
# Bibliography

# Bibliography

1 Meteotest, "METEONORM Version 6.1 - Edition 2009," 2008.

2 National Climatic Data Center (NCDC), *Typical Meteorological Year User's Manual TD-9734, Hourly Solar Radiation - Surface Meteorological Observations*. Asheville: National Climatic Data Center, U.S. Department of Commerce, 1981.

3 European Commission, *Test Reference Years, Weather data sets for computer simulations of solar energy systems and energy consumption in buildings*, *CEC DG XII*. Brussels: European Comission, 1985.

4 National Climatic Data Center (NCDC), *Test reference year (TRY) DSI-9706*. Asheville: National Climatic Data Center, U.S. Department of Commerce, 1976.

5 ASHRAE, *Weather year for energy calculations*. Atlanta: : American Society of Heating, Refrigerating and Air-Conditioning Engineers, Inc., 1985.

6 G. N. Walton, *Thermal analysis research program reference manual*. Washington: U.S. Department of Commerce, National Bureau of Standards, 1983.

7 M. Martin and P. Berdahl, "Characteristics of infrared sky radiation in the United States," *Solar Energy*, vol. 33, pp. 321–336, 1984.

8 P. Berdahl and F. Fromberg, "The thermal radiance of clear skies," *Solar Energy*, vol. 29, pp. 299–314, 1982.

9 P. Berdahl and M. Martin, "Emissivity of clear skies," *Solar Energy*, vol. 32, pp. 663–664, 1984.

10 F. Kasten and G. Czeplak, "Solar and terrestrial radiation dependent on the amount and type of cloud," *Solar Energy*, vol. 24, pp. 177–189, 1979.

11 M. Perraudeau, "Daylight availbility from energetic data," in *CIE Daylighting conference Vol.I*, (Moscow), p. A17, 1990.

12 R. H. van Gent, "on the History of Astronomy," 2011.

13 J. W. Spencer, "Fourier series representation of the position of the sun," *Search*, vol. 2, no. 5, p. 172, 1971.

14 J. A. Duffie and W. A. Beckman, *Solar engineering of thermal processes*. New York: John Wiley & Sons Inc, first ed ed., 1980.

15 M. Iqbal, *An introduction to solar radiation*. New York - London: Academic Press Inc, 1983.

16 R. Perez, R. Stewart, C. Arbogast, R. Seals, and J. Scott, "An isotropic hourly diffuse radiation model for sloping surfaces: Description, performance validation, site dependecy evaluation," *Solar Energy*, vol. 36, no. 6, pp. 481–497, 1986.

17 R. Perez, R. Seals, P. Ineichen, R. Stewart, and D. Meniucci, "A new simplified version of the Perez diffuse irradiance model for tilted surfaces," *Solar Energy*, vol. 39, no. 3, pp. 221–231, 1987.

18 T. Defraeye, B. Blocken, and J. Carmeliet, "Convective heat transfer coefficient for exterior building surfaces: Existing correlations and CFD modelling," *Energy Conversion and Management*, vol. 52, no. 1, pp. 512–522, 2011.

19 W. Jürges, "Der Wärmeübergang an einer ebenen Wand," *Beihefte zum Gesundheits-Ingenieur*, vol. 1, no. 19, 1924.

20 J. Stefan, "Über die Beziehung zwischen der Wärmestrahlung und der Temperatur," *Sitzungsberichte der mathematisch-naturwissenschaftlichen Classe der kaiserlichen Akademie der Wissenschaften*, vol. 79, pp. 391–428, 1879.

21 L. Boltzmann, "Ableitung des Stefan'schen Gesetzes, betreffend die Abhängigkeit der Wärmestrahlung von der Temperatur aus der electromagnetischen Lichttheorie," *Annalen der Physik und Chemie*, vol. 22, pp. 291–294, 1884.

22 P. J. Mohr, B. N. Taylor, and D. B. Newell, "CODATA Recommended values of the fundamental physical constants: 2006," *Reviews of Modern Physics*, vol. 80, pp. 633–730, 2008.

23 D. C. Hamilton and W. R. Morgan, "Radiant-interchange configuration factors," tech. rep., National Advisory Comittee for Aeronautics, Washington, 1952.

24 A. J. N. Khalifa, "Ntural convective heat transfer coefficient - a review : Surfaces in two- and three-dimensional enclosures," *Energy Conversion and Management*, vol. 42, no. 4, pp. 505–517, 2001.

25 H. B. Awbi and A. Hatton, "Natural convection from heated room surfaces," *Energy and Buildings*, vol. 30, no. 3, pp. 233–244, 1999.

26 I. Beausoleil-Morrison, *The adaptive coupling of heat and air flow modeling within dynamic whole-building simulation*. PhD thesis, 2000.

27 H. Buchberg, *Electric analogue prediction of thermal behavior of an inhabitable enclosure*. Msc, University of California, 1954.

28 H. Buchberg, "Electric analogue prediction of thermal behavior of an inhabitable enclosure,"

*ASHRAE Transactions*, vol. 61, pp. 339–386, 1955.

29  A. K. Oppenheim, "Radiation analysis by the network method," *Transactions of American society of mechanical engineers*, vol. 78, pp. 725–735, 1956.

30  A. E. Kenelly, "Equivalence of triangles and stars in conducting networks," *Electrical World and Engineer*, vol. 34, pp. 413–414, 1899.

31  R. J. Liesen and C. O. Pedersen, "An evaluation of inside surface heat balance models for cooling load calculations," *ASHRAE Transactions*, vol. 103 Part 2, pp. 485–502, 1997.

32  E. U. Finlayson, D. K. Arasteh, C. Huizenga, M. D. Rubin, and M. S. Reilly, "WINDOW 4.0: Documentation of calculation procedures," tech. rep., 1993.

33  D. K. Arasteh, J. Hartmann, and M. Rubin, "Experimental verification of a model of heat transfer through windows," *ASHRAE Transactions*, vol. 93, no. 1, pp. 1425–1431, 1986.

34  R. A. Furler, P. Williams, and F. K. Kneubühl, "Experimental and theoretical studies on the energy balance of windows - NEFF Project report 177.1," tech. rep., 1988.

35  R. A. Furler, "Angular dependence of optical properties of homogeneous glasses," *ASHRAE Transactions*, vol. 97, no. 2, 1991.

36  M. A. Fresnel, "Mémoire sur la diffraction de la lumière," *Mémoires de l'Académie des Sciences (Paris)*, vol. 5, pp. 33–475, 1926.

37  V. Snellius, *Doctrina triangulorum.* 1627.

38  M. Koschenz and B. Lehman, *Thermoaktive Bauteilsysteme tabs.* Dübendorf: EMPA-Akademie, 2000.

39  W. De Soto, S. Klein, and W. Beckman, "Improvement and Validation of a Model for Photovoltaic Array Performance," *Solar Energy*, vol. 80, pp. 78–88, 2006.

40  D. Sera, R. Teodorescu, and P. Rodriguez, "PV panel model based on datasheet values," in *IEEE International Symposium on Industrial Electronics*, pp. 2392–2396, 2007.

41  E. Haesen, *Multi-Objective Optimization of the Integration of Stochastic Distributed Energy Resources in Electricity Grids.* PhD thesis, 2009.

42  H. Willis, *Power Distribution Planning Reference Book.* 2004.

43  W. Kersting, "Radial Distribution Test Feeders," in *IEEE Power Engineering Society Winter Meeting*, (Columbus, Ohio), pp. 908–912, 2001.